



Facile synthesis of N-doped carbon dots/g-C₃N₄ photocatalyst with enhanced visible-light photocatalytic activity for the degradation of indomethacin



Fengliang Wang^a, Ping Chen^a, Yiping Feng^a, Zhijie Xie^a, Yang Liu^b, Yuehan Su^a, Qianxin Zhang^a, Yingfei Wang^a, Kun Yao^a, Wenying Lv^a, Guoguang Liu^{a,*}

^a School of Environmental Science and Engineering, Institute of Environmental Health and Pollution Control, Guangdong University of Technology, Guangzhou 510006, China

^b Faculty of Environmental & Biological Engineering, Guangdong University of Petrochemical Technology, Maoming 525000, China

ARTICLE INFO

Article history:

Received 2 November 2016

Received in revised form 19 January 2017

Accepted 7 February 2017

Available online 8 February 2017

Keywords:

N-doped carbon dots

Graphitic carbon nitride

IDM

Degradation pathways

ABSTRACT

In this study, a novel visible-light-driven N-doped carbon dot (NCDs)/g-C₃N₄ composite was successfully synthesized by loading NCDs nanoparticles onto the interlayers and surface of g-C₃N₄ via a facile polymerized method. The photocatalytic activity of the NCDs/g-C₃N₄ was remarkably higher than that of g-C₃N₄ and CDs/g-C₃N₄ toward the degradation of indomethacin (IDM) under visible light irradiation. With increasing NCDs loading volumes, the photocatalytic activity of NCDs/g-C₃N₄ initially increased, and then decreased. A very low NCDs content of 1.0 wt% resulted in a 13.6 fold higher reaction rate than that of pristine g-C₃N₄. This enhanced photocatalytic activity might have been ascribed to the unique up-converted PL properties, efficient charge separation, as well as bandgap narrowing of the NCDs. Reactive species (RS) scavenging experiments revealed that superoxide radical anions (O₂^{•-}) and photogenerated holes (h⁺) played key roles during the photocatalytic degradation of IDM. The quantification of O₂^{•-} showed that NCDs/g-C₃N₄ formed a larger amount of O₂^{•-} than that of pristine g-C₃N₄. Potential photocatalytic pathways of IDM were proposed through the identification of intermediates using HPLC-MS/MS and the prediction of reaction sites based on Frontier Electron Densities (FEDs) calculations, which involved decarboxylation, hydroxylation, as well as the addition and cleavage of indole rings. Toxicity and mineralization evaluations revealed that NCDs/g-C₃N₄ provided a very desirable performance for the toxicity reduction and mineralization of IDM under longer exposures of visible light irradiation.

© 2017 Elsevier B.V. All rights reserved.

1. Introduction

Graphitic carbon nitride (g-C₃N₄) with a suitable visible light-driven band gap (2.7 eV) is a metal-free polymeric photocatalyst, which has been considered to be a safe catalyst [1,2]. Although g-C₃N₄ is believed to be a superior visible-light photocatalyst for pollutant degradation, CO₂ reduction, and hydrogen production [3], the high recombination rates of photo-generated electron-hole pairs and low visible-light absorption efficiencies limit the photocatalytic efficacy of pristine g-C₃N₄ [4], which greatly hinder its practical applications. To date, many strategies including doping

with metal-ions (e.g., Ag and Cu) [5,6], and combining with other semiconductors (e.g., Cu₂O) [7], have been employed to reduce the band gap and extend the absorption band of g-C₃N₄ for improving its photocatalytic performance. However, the leakage of doped metals from composite material in this application may enhance the toxicity of the photo-catalyst [8]. Therefore, environmentally compatible modifying materials are required to improve the photocatalytic efficiency of g-C₃N₄.

Carbon dots (CDs), comprise a novel type of carbon-based nanomaterial with dimensions of below 10 nm, which have attracted widespread interest due to their unique properties [8]. Due to their fascinating properties, CDs have been successfully integrated with semiconductors to improve their photocatalytic activity [9–11], by decreasing electron-hole recombination events and broadening the photo-absorption region. The conjugated π structure of CDs may enhance interactivities between CDs and semiconductors, result-

* Corresponding author at: School of Environmental Science and Engineering, Guangdong University of Technology, No. 100 Waihuan Xi Road, Guangzhou Higher Education Mega Center, Guangzhou 510006, China.

E-mail address: liugg615@163.com (G. Liu).

ing in a stable composite. Recently, CDs modified g-C₃N₄ has been reported as an efficient photocatalyst for H₂ evolution [12,13], as well as the degradation of methyl orange [14], RhB [13,15], tetracycline hydrochloride [15], and phenol [8]. In addition, N-doped nanostructured carbon materials are of great interest because of their improved electron transfer and extension of the visible light adsorption region through doping with N atoms [16,17]. However, to the best of our knowledge, NCDs modified g-C₃N₄ has never been reported.

In recent years, pharmaceutical and personal care products (PPCPs) have emerged as contaminants that have attracted increasing concern [18,19]. It has been demonstrated that exposure to PPCPs has negative impacts in human health as well as for ecosystems [20]. Due to their stable chemical structures and recalcitrance to biological degradation, conventional water treatment processes are not always efficient in the removal of PPCPs [21]. As a result, they have been frequently detected across a wide range of aquatic environments, including surface water, groundwater, and potable water [22]. Consequently, the development of efficient methods for the treatment of water resident PPCPs is of critical urgency.

In this study, a NCDs/g-C₃N₄ photocatalyst was synthesized through a facile hydrothermal-polymerized method, and applied to the degradation of PPCPs under visible light irradiation. The structural and optical properties of composite were investigated. Indomethacin (IDM) is a non-steroidal anti-inflammatory drug commonly used for the treatment of rheumatoid arthritis [23], which was studied as representative of PPCPs. The effects of NCDs content and N-doping concentrations of NCDs on the properties of the NCDs/g-C₃N₄ composite were evaluated. The efficiency of the NCD/g-C₃N₄ composite on the degradation of IDM was quantified, and the mechanism of enhanced photocatalytic activity was deduced. Additionally, potential IDM photodegradation pathways were proposed based on products identification by HPLC–MS/MS, as well as theoretical FED calculations. Subsequently, changes in toxicity and mineralization during the photocatalytic degradation of IDM were evaluated.

2. Materials and methods

2.1. Materials

Indometacin (IDM, 98% purity) was purchased from TCI Reagent Co. Ltd. (China). Dicyandiamide, potassium superoxide (KO₂) and 4-chloro-7-nitrobenzo-2-oxa-1,3-diazole (NBD-Cl) were obtained from Aladdin (China). HPLC-grade acetonitrile and methanol were obtained from CNW Technologies GmbH (Germany). Analytical grade citric acid, urea, benzoquinone, isopropanol, sodium azide, Na₂C₂O₄, K₂Cr₂O₇, acetic acid, and sulfuric acid were purchased from Taitan (China). Deionized (DI) water from a Milli-Q apparatus (Germany) was used throughout this study.

2.2. Preparation of photocatalysts

2.2.1. Preparation of NCDs and CDs

N-doped carbon dots (NCDs) were synthesized via a hydrothermal method [24]. In a typical procedure, 3.0 g of citric acid was combined with a certain quantity of urea (0.5, 1.0, 2.0, and 3.0 g) and dissolved in 15 mL of DI water. The mixture was then transferred to a Teflon-sealed autoclave and heated at 180 °C for 5 h. After cooling to room temperature, the obtained brown solution was centrifuged at 10,000 rpm for 30 min to remove large particles. The solution was then adjusted to a neutral pH with a HCl solution to obtain the NCDs solution. The NCDs solution was dried overnight at 70 °C to obtain the NCDs powder. Following the same procedure, N-free CDs were also synthesized with citric acid as the

only precursor. Finally, the obtained NCDs and N-free CDs powders were fully suspended in DI water through ultrasonication to obtain the stock solutions (20 g/L).

2.2.2. Preparation of g-C₃N₄

Graphitic carbon nitride (g-C₃N₄) was prepared by directly heating dicyandiamide [1]. Typically, 5.0 g of dicyandiamide was introduced into an alumina crucible with a cover, and then heated to 550 °C for 3 h at a heating rate of 2.8 °C/min. Subsequent to cooling to room temperature, the obtained bulk g-C₃N₄ was milled into powders.

2.2.3. Preparation of NCDs/g-C₃N₄ photocatalyst

The NCDs/g-C₃N₄ was synthesized via a facile polymerization method. In a typical experiment, 3.0 g of dicyandiamide was dissolved in 20 mL of DI water, which contained a certain quantity of NCDs. After mixing mechanically, the mixture was carefully vaporized at 70 °C. The obtained powder was subsequently heated to 550 °C for 3 h at a heating rate of 2.8 °C/min. After cooling to room temperature, the resultant yellow powder was collected through filtration. Different NCDs/g-C₃N₄ samples with NCDs at mass percentages of 0.0%, 0.1%, 0.5%, 1.0%, 1.5%, and 2.0% were prepared through the same procedure. Similarly, 1.0 wt% of CDs/g-C₃N₄ was prepared by the same route.

2.3. Characterization of photocatalysts

A scanning electron microscope (SEM, JSM-6700) equipped with energy dispersive spectroscopy (EDS) and a transmission electron microscope (TEM, JEM-2100HR) were employed to observe the microscopic morphology of the samples. The crystal structure of the obtained materials was characterized by X-ray diffraction (XRD, BRUKER D8 ADVANCE) with Cu K α radiation ($\lambda = 0.154178$ nm). The UV-vis absorption spectra of the as-prepared photocatalysts were recorded via a UV2450 UV-vis spectrophotometer (Shimadzu) using BaSO₄ as a reflectance standard. X-ray photoelectron spectroscopy (XPS) was used to analyze the ionic characteristics, which was achieved on a Thermo VG ESCALAB 250 spectrometer with Al K α radiation at 1486.6 eV. Fourier transform infrared (FT-IR) spectra were performed using a Nicolet 6700 spectrophotometer (Thermo Fisher) with the samples dispersed in KBr. Photoluminescence (PL) spectra were measured with a FluoroMax-4 fluorescence spectrophotometer (HORIBA Jobin Yvon).

2.4. Photocatalytic activity tests

2.4.1. Photocatalytic experiments

Photocatalytic activity tests of the NCDs/g-C₃N₄ were evaluated via the photocatalytic degradation of IDM under visible light. The experiment was carried out in a XPA-7 rotary photochemical reactor (Fig. S1, Nanjing Xujiang machine plant). A 350 W xenon lamp with a 420 nm cut-off filter, a 500 W mercury lamp, a 350 W xenon lamp with a 290 nm cut-off filter, and a 9 w monochromatic light lamp with the wavelength of 850 nm (Shenzhen lamplic co., LTD.) were employed as the visible light irradiation source, the UV light irradiation source, the simulated sunlight irradiation source, and near-infrared light source, respectively. For each experiment, 50 mL of a 4 mg/L IDM aqueous solution containing 1.0 g/L catalysts were introduced into a 50 mL quartz tube, and adjusted to a neutral pH with 1% NaOH or H₂SO₄ solution. Prior to light irradiation, the reaction solution was agitated in the dark for 30 min to obtain adsorption equilibrium for IDM on the photocatalyst. During the photocatalytic process, 1.0 mL samples were extracted at predetermined time intervals, and filtered through 0.22 μ m Millipore filters in order to remove the nanophotocatalyst. The residual IDM

in solution was analyzed by high performance liquid chromatography (HPLC). The detailed analytical method is conveyed in the Text S1. The total organic carbon (TOC) of the reaction solutions were measured via a TOC analyzer (TOC-V CPH E200V, Shimadzu Co., Japan).

2.4.2. Photocatalytic efficiency

The photocatalytic efficiencies of photocatalyst is determined by the measurement of the apparent photonic efficiency [25,26], defined as

$$\xi_x(\%) = \frac{r_{IDM} (\text{mol} \cdot \text{L}^{-1} \cdot \text{min}^{-1})}{I_{hv} (\text{Einstein} \cdot \text{min}^{-1})} \times 100$$

where r_{IDM} is the reaction rate of IDM and I_{hv} is the incident photon flux (6.02×10^{-7} Einstein min $^{-1}$) determined by chemical actinometry using potassium ferrioxalate [27].

2.4.3. Determination of RSs during photocatalytic degradation

RSs scavenging experiments were employed to ascertain the reactive species in the IDM photodegradation process. Benzoquinone (BQ), 10 mM isopropanol (IPA), 75 mM sodium azide (NaN₃), 10 mM Na₂C₂O₄, and 50 μM K₂Cr₂O₇ were used as the superoxide iron radical (O₂^{•-}), hydroxyl radical (·OH), singlet oxygen (¹O₂), photogenerated hole (h⁺), and photogenerated electron (e⁻) scavenger, respectively [28–30].

In order to quantitatively determine the concentration of O₂^{•-}, 200 μmol/L NBD-Cl was used as the fluorescent probe [31,32]. The identification of the NBD-Cl product (reaction product of O₂^{•-} and NBD-Cl) was conducted by recording a fluorescence emission spectrum at 550 nm (excited at 470 nm). The NBD-Cl concentration was measured by its absorbance at a 342 nm wavelength using a UV-vis spectrophotometer.

2.4.4. Identification of photocatalytic by-products

Photodegradation intermediates of IDM were identified using liquid chromatography with tandem mass spectrometry (HPLC-MS/MS), which is detailed in the Text S1.

2.5. Acute toxicity test

The photobacterium phosphoreum was employed to measure acute toxicity, which was conducted via a Microtox Model DXY-2 Toxicity Analyzer [33]. The inhibition (I) of *V. fischeri* was calculated based on Eq. (1) where I_{sample} and I_{blank} were the luminosity of the sample solution and the blank solution without IDM and nitrate, respectively.

$$I = \left(1 - \frac{I_{\text{sample}}}{I_{\text{blank}}} \right) \times 100 \quad (1)$$

2.6. Theoretical calculation

Molecular orbital calculations were derived through the B3LYP/6-311G+(d, p) level with the optimal conformation having a minimum energy obtained in the Gaussian 09 program. The optimized structure and atomic numbering of indomethacin is depicted in Fig. S2. The frontier electron densities (FEDs) of the highest occupied molecular orbital (HOMO) and the lowest unoccupied molecular orbital (LUMO) were determined. According to the Frontier Orbital Theory, ·OH typically attacks the sites with higher FED²_{HOMO}+FED²_{LUMO} values, while positions with a more positive point charge were more easily attacked by O₂^{•-} [34,35].

3. Results and discussion

3.1. Characterization

3.1.1. Characterization of N-doped carbon dots

Fig. 1a shows the UV-vis absorptions of NCDs and CDs in an aqueous solution, where NCDs exhibit a broader UV-vis absorption than CDs in the range of from 300 nm to 400 nm. NCDs also show two intrinsic peaks, centered at 250 nm and 350 nm, which may respectively be attributed to the π-π* transition of aromatic sp₂ conjugate domains and the n-π* transitions of C=O bands [36–38]. Fluorescence tests indicated that NCDs demonstrated a brighter blue emission than CDs under 365 nm UV lamp irradiation (Fig. S3a), which might have been attributed to the reduction of the non-radiation recombination center by the doping of amino groups on the NCDs surface [38]. Furthermore, the optical properties measurement of the PL presents the superior up-converted photoluminescence property of the NCDs (Fig. 1b). As the NCDs were excited by long-wavelength light, from 650 nm to 900 nm, the up-converted emissions were remarkably located in the range of from 400 nm to 700 nm were shown. The above results implied that the NCDs might enhance the photocatalytic efficiency through the conversion of near-infrared emission wavelength to visible light, which enabled it to be employed as a powerful energy transfer component in the design of the photocatalyst.

The TEM image in Fig. 1c reveals the spherical morphology of NCDs. The average diameter of NCDs was ca. 2.5 nm (Fig. S3b). HRTEM image (inset of Fig. 1c) clearly displays the crystalline structure of the NCDs, with lattice spacing of 0.22 nm, agreeing well with the (100) lattice planes of graphite [39], which indicated that the NCDs possessed a crystalline graphitic carbon structure. The XRD pattern of NCDs in Fig. 1d shows a broad peak at ~2θ = 24.0° with an interlayer spacing of 0.37 nm, which was larger than that of graphite (0.34 nm) [40]. The increase in interlayer spacing may be attributed to the introduction of oxygen-containing functional groups on the NCDs [41].

FT-IR analysis in Fig. 2a exhibited several peaks at 1647 cm⁻¹ (C=N), 1425 cm⁻¹ (C=O), 1380 cm⁻¹ (-NH), 1209 cm⁻¹ (C-N), 1108 cm⁻¹ (C-NH-C), 1043 cm⁻¹ (-C-O-C-) and 3430 cm⁻¹ (C-OH and N-H) on the surface of NCDs [36,42,43]. Various polar groups (hydroxyl, carboxyl, carbonyl, and epoxy groups) existed on the surface of the NCDs which both improved the solubility and stability of NCDs, as well as enhanced the electron donation and acceptance capability of the NCDs [39].

The XPS spectra in Fig. 2b shows the existence of carbon (C1s, 284.1 eV), nitrogen (N1s, 400.1 eV), and oxygen (O1s, 532.0 eV) on the surface of the NCDs. Fig. 2c-d and Fig. S4 present the high-resolution XPS spectra of C1s, N1s, and O1s. C1s may be split into three peaks at 284.5, 286.0, and 288.4 eV, which may be assigned to C=C, C=O, and C-N, respectively [44,45]. The N1s may be deconvoluted to two peaks at 399.1, 400.3 and 400.3 eV, corresponding to the C-N-C and N-(C)₃ [40,43]. The C1s and N1s analysis demonstrated that N atoms were involved in the carbon cores of CDs through chemical bonds. The O1s peaks with binding energies of 531.7 and 532.9 eV were assigned to the C=O and C-OH/C-O-C [46]. The XPS results confirmed the successful preparation of NCDs, which possessed a variety of chemical groups, including amide, hydroxyl, and carboxyl on its surface. These chemical groups mainly came from the precursor citric acid and urea [47]. Based on the FT-IR and XPS results and the previous researches [47,48], the formation mechanism of NCDs was proposed (Fig. S5). First citric acid self-assembled into a nanosheet structure, then a graphene nanoparticles with carboxyl- and hydroxyl-groups were formed via the dehydrolysis process under hydrothermal conditions. Sub-

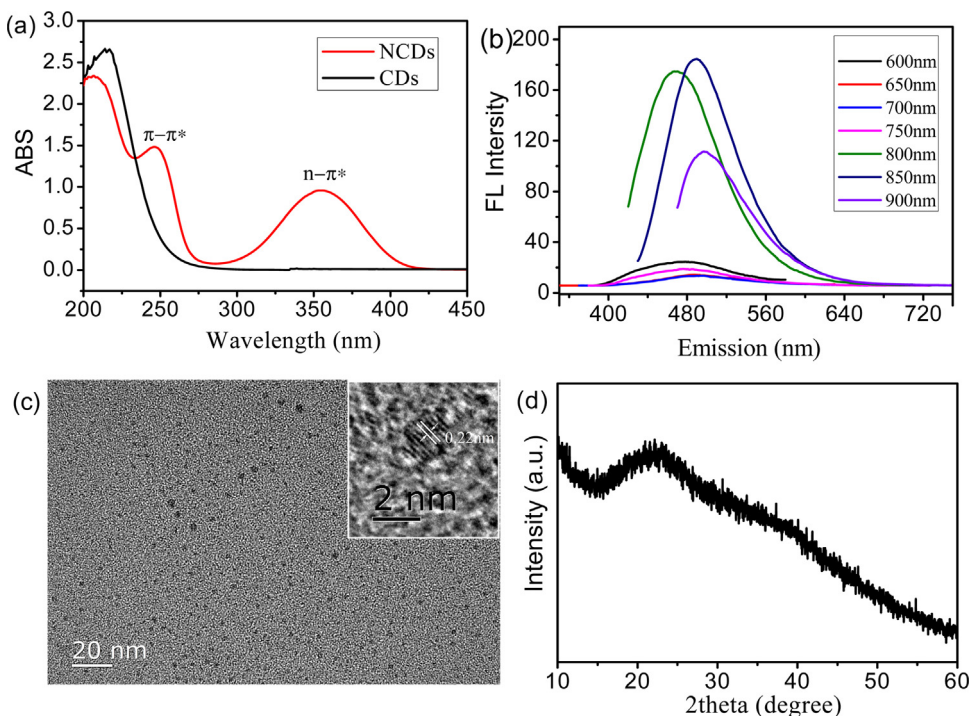


Fig. 1. (a) UV-vis absorption spectra of the CDs and NCDs; (b) Up-converted photoluminescence spectra of NCDs; (c) TEM image of NCDs. Inset shows the HRTEM of NCDs. (d) XRD spectrum of NCDs.

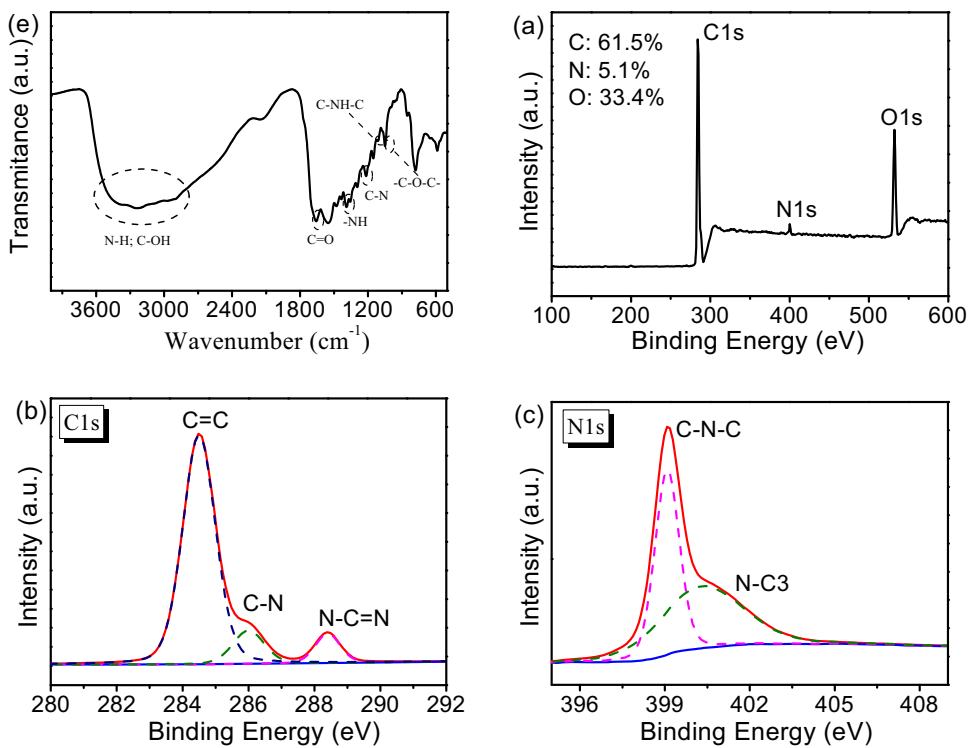


Fig. 2. (a) FT-IR spectrum of NCDs. (b) XPS survey spectra of NCDs. (c) High-resolution XPS spectra of C1s, and (d) N1s regions.

sequently, amination happened to formed NCDs in the present of urea.

3.1.2. Characterization of NCDs/g-C₃N₄ composite

The TEM images in Fig. 3a–b reveal the 2D lamellar structure of g-C₃N₄. Fig. 3c–f depicts the attachment of NCDs on the surface and interlayer of g-C₃N₄. The EDS displayed in Fig. S6 demonstrates that

nitrogen (N) and carbon (C) were the primary elements of NCDs/g-C₃N₄.

Fig. S7 shows that two distinct diffraction peaks at $2\theta = 27.5^\circ$ and 13.0° of NCDs/g-C₃N₄ are perfectly indexed to pure g-C₃N₄ (JCPDS Card No. 87-1526), which revealed that the NCDs doping did not significantly alter the crystal structure of g-C₃N₄. The stronger diffraction peak at $2\theta = 27.5^\circ$ may be indexed to (002) planes with

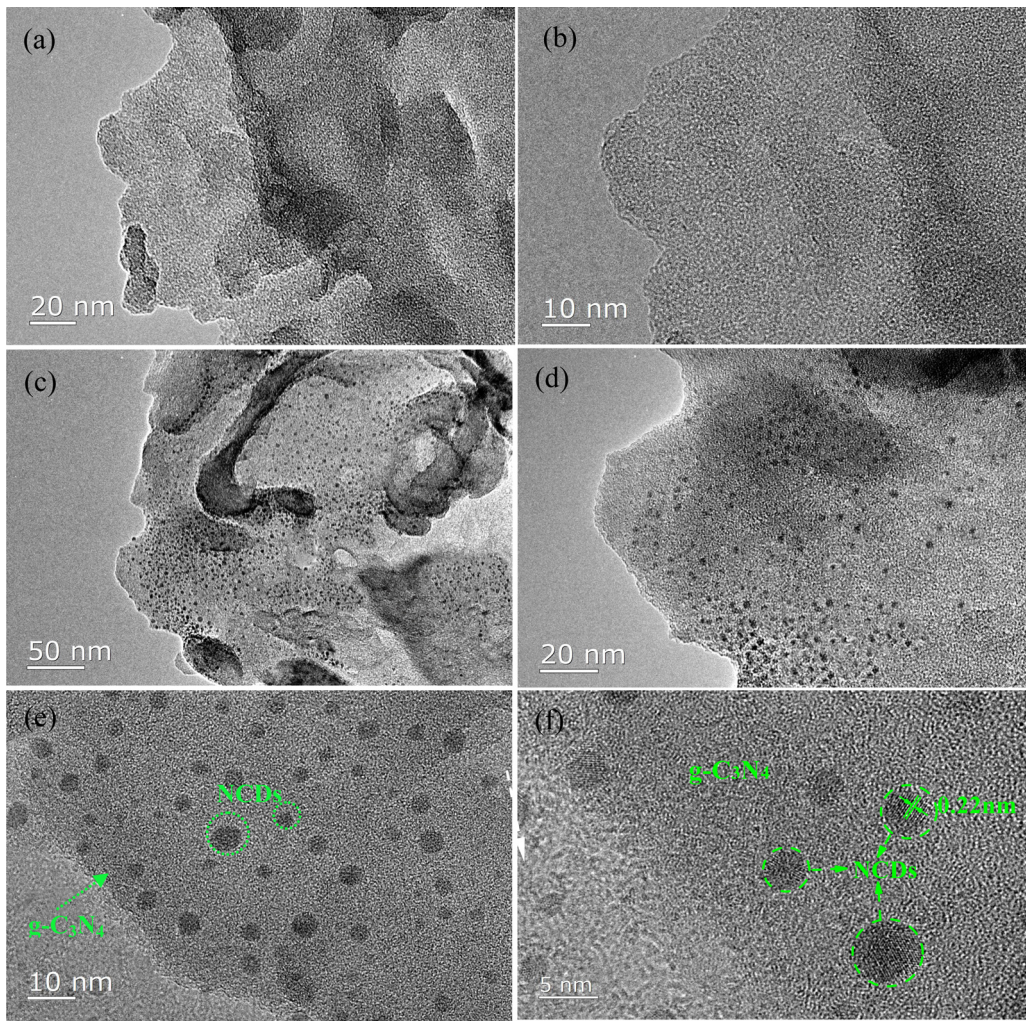


Fig. 3. (a and b) TEM images of g-C₃N₄; (c–e) TEM image of NCDs/g-C₃N₄; (f) HRTEM image of NCDs/g-C₃N₄.

an interlayer spacing of ~0.325 nm, corresponding to the characteristic interlayer stacking structure of aromatic segments [49]. The weaker of these at 20=13.0° may be indexed to the (100) peak with an interlayer spacing of ~0.680 nm, relating to the in-plane structural packing motif of tri-s-triazine units [50]. Moreover, no NCDs diffraction peaks were observed in the NCDs/g-C₃N₄ due to the small quantity and low crystallinity of NCDs [38].

From the FT-IR spectrum of g-C₃N₄ in Fig. 4a, vibration peaks at from between 1200 cm⁻¹ and 1650 cm⁻¹ can be seen, which can be attributed to typical CN heterocycle stretching modes [51,52]. The band at 810 cm⁻¹ corresponds to triazine units [8,53], whereas the wider band at ~3430 cm⁻¹ corresponds to C—OH and N—H stretching vibrations [1]. For NCDs/g-C₃N₄, a new bending vibration at 2918 cm⁻¹ (C—H) was observed, and the 1434 cm⁻¹ peak became stronger. These FT-IR results indicated that the NCDs were successfully coated onto the g-C₃N₄ surface.

The XPS spectra depicted in Figs. Fig. 4b and S8 reveals the presence of C, N, and O in both g-C₃N₄ and NCDs/g-C₃N₄ samples. The C1s for g-C₃N₄ were divided into two species: C=C (284.6 eV, 5.5%) and N—C=N (288.0 eV, 94.5%), respectively [28,54]. Subsequent to NCD doping, a new peak at 285.6 eV (0.48%) corresponding to the C—OH and associated with the NCDs was observed [8]. The N1s of g-C₃N₄ may be separated into four peaks at 398.6, 400.0, 401.1, and 404.1 eV, which are attributed to triazine rings, N—(C)₃ groups, N—H, and graphitic species [28,55]. Similarly, the O1s peak of pure g-C₃N₄ and NCDs/g-C₃N₄ may be divided into two peaks at 531.8

and 533.3 eV, which can be assigned to C=O and C—OH/C—O—C bonds [36,37]. Of note is that the peak at ca. 531.8 eV could be ascribed to C=O, which increased from 55.4% to 61.7% due to a significant population of NCDs resident carboxyl groups.

The UV-vis diffuse reflectance spectra (DRS) of g-C₃N₄ and NCDs/g-C₃N₄ are depicted in Fig. 4c. Pristine g-C₃N₄ reveals a distinct absorption band at ~475 nm, which was consistent with previous reports [29]. In contrast to g-C₃N₄, the NCDs/g-C₃N₄ demonstrated an obvious red-shift and showed strong absorption in the visible light band. Moreover, the absorption gradually increased in alignment with the additional NCDs content. To further study the optical properties of NCDs/g-C₃N₄, the optical band gaps were obtained according to Eq. (2)

$$(\alpha h\nu)^{1/2} = A(h\nu - Eg) \quad (2)$$

As illustrated in the inset of Fig. 4c, g-C₃N₄ presents a band gap of 2.62 eV, which is close to that reported in previous literature [1]. Following the loading of NCDs, the NCDs/g-C₃N₄ exhibited a significantly reduced band gap. The energy band structure parameters were listed in Table S1. This reduction might be explained by the additional electronic state above the valence band of g-C₃N₄ [56].

Subsequently, PL analysis was conducted to investigate the separation efficiency of photogenerated electrons and holes. A lower fluorescence emission intensity indicated a reduced electron–hole recombination rate, and higher photocatalytic activity [13,57]. The PL emission spectrum of pristine g-C₃N₄ in Fig. 4d displays a strong

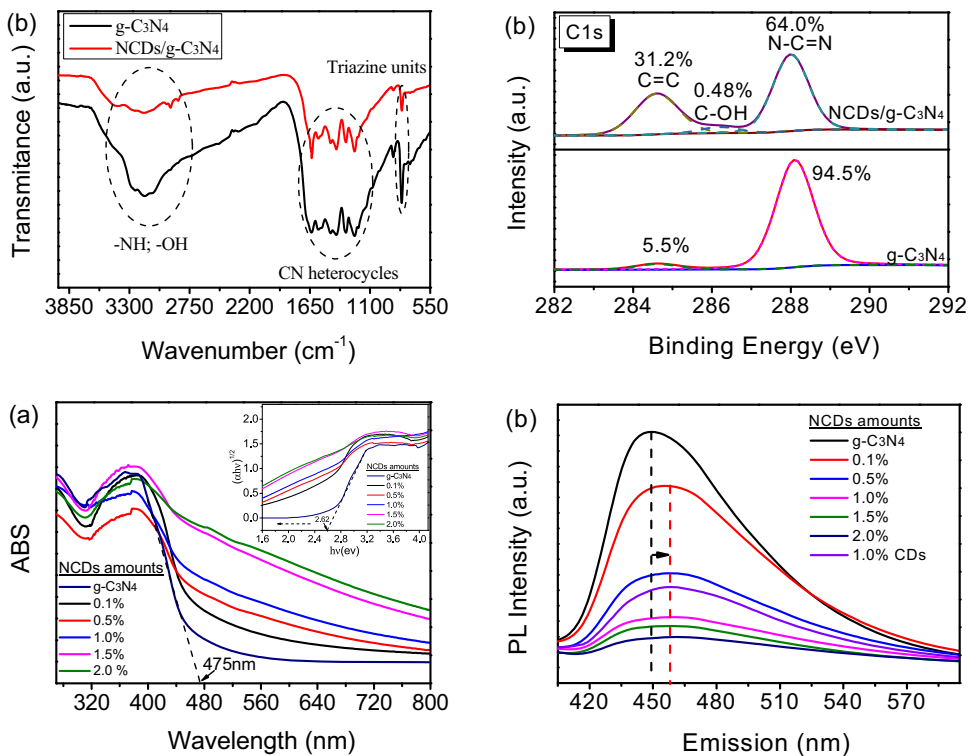


Fig. 4. (a) FT-IR spectrum of g-C₃N₄ and NCDs/g-C₃N₄. (b) High-resolution XPS spectrum of g-C₃N₄ and NCDs/g-C₃N₄. (c) UV-vis diffuse reflectance absorbance spectra of g-C₃N₄ and NCDs/g-C₃N₄. (Inset: The band gap of g-C₃N₄ and NCDs/g-C₃N₄ determined from the $(ahv)^{1/2}$ versus photon-energy.) (d) PL spectra of g-C₃N₄, NCDs/g-C₃N₄ and CDs/g-C₃N₄ under 380 nm excitation.

emission peak at ~450 nm when excited at a wavelength of 375 nm. Compared to g-C₃N₄, the PL intensity of the NCDs/g-C₃N₄ composites decrease remarkably, indicating that the doping of NCDs might promote the transfer of charges and inhibit the electron-hole recombination rate. Further, the emission peak of the NCDs/g-C₃N₄ showed an obvious red-shift of from 444 nm to 455 nm. Moreover, the peak at 455 nm of the NCDs/g-C₃N₄ composites was obviously weaker than that of the CDs/g-C₃N₄, which implied a remarkable improvement in electron transfer due to N atom doping. This enhancement in electron transfer can be attributed to the electron-withdrawing ability of N atoms within the conjugated C plane [58–60].

In summary, it may be concluded that the presence of NCDs can improve the absorbance of g-C₃N₄ in the visible region, as well as enhance its electron transfer capacity. Further, the up-conversion ability of NCDs enabled them to convert long wavelengths of light to shorter wavelengths, which can be absorbed by g-C₃N₄. The superior properties of NCDs resulted in the enhancement of the photocatalytic activities of the NCDs/g-C₃N₄ composite.

3.2. Photocatalytic activity of NCDs/g-C₃N₄ composite

3.2.1. Enhanced photocatalytic activity of NCDs/g-C₃N₄ under visible light irradiation

The photocatalytic activity of the as-prepared NCDs/g-C₃N₄ was evaluated for the degradation of IDM under visible light irradiation (Fig. 5a). IDM cannot be decomposed in the absence of a photocatalyst, which indicates that IDM is resistant to photodegradation under visible light irradiation. The adsorption experiment shows that only 5.3% IDM can be absorbed by NCDs/g-C₃N₄ during the photocatalytic process; however, obvious IDM decomposition has been observed in the presence of g-C₃N₄. The NCDs/g-C₃N₄ composite indicated significantly more rapid degradation than through the use of pure g-C₃N₄. With pristine g-C₃N₄, ca. 16.0% of the IDM

was decomposed following 90 min of treatment, while 91.5% of the IDM was degraded via the composite that contained 1.0 wt% NCDs over the same timeline. The apparent photonic efficiencies of g-C₃N₄ and NCDs/g-C₃N₄ were calculated to be 3.65% and 49.3%, respectively. Thus, 135.1% increase in the photonic efficiency was observed for the NCDs/g-C₃N₄. These results indicated that the NCDs played a critical role in the enhancement of the photocatalytic activity of g-C₃N₄. In addition, the photocatalytic activity of NCDs/g-C₃N₄ was markedly superior to a physical mixture of NCDs and g-C₃N₄, which revealed a synergistic catalytic effect of the NCDs/g-C₃N₄ composite.

3.2.2. Effects of the quantity of NCDs on photocatalytic activity

Fig. 5b depicts the kinetic rate constant of IDM degradation by the NCDs/g-C₃N₄ composite using different quantities of NCDs under visible light irradiation. The rate constant of IDM gradually increased with larger quantities of NCDs, from 0.0 wt% to 1.0 wt%. Optimal activity (0.0272 min^{-1}) was obtained with 1.0 wt% NCDs/g-C₃N₄, which was ca. 13.6 times higher than pristine g-C₃N₄ (0.0020 min^{-1}). However, further NCDs loading increases (>1.0 wt%) resulted in decreased degradation rates, which might be attributed to the NCDs inner filter effect via competition for the absorption of photons with g-C₃N₄; thereby reducing the formation of reactive species [51].

3.2.3. Effects of the quantity of urea on photocatalytic activity

The photocatalytic activity of a NCDs/g-C₃N₄ composite prepared with different quantities of urea was investigated (Fig. 5c). The NCDs/g-C₃N₄ prepared with urea showed a higher photocatalytic activity than the N-free CDs/g-C₃N₄. With increasing amounts of urea, from 0.0 to 1.0 g, the photocatalytic activity increased from 0.014 to 0.027 min^{-1} . However, as the amount of urea was further increased (1.0–3.0 g), the photocatalytic activity was observed to decrease significantly ($0.027\text{--}0.017 \text{ min}^{-1}$).

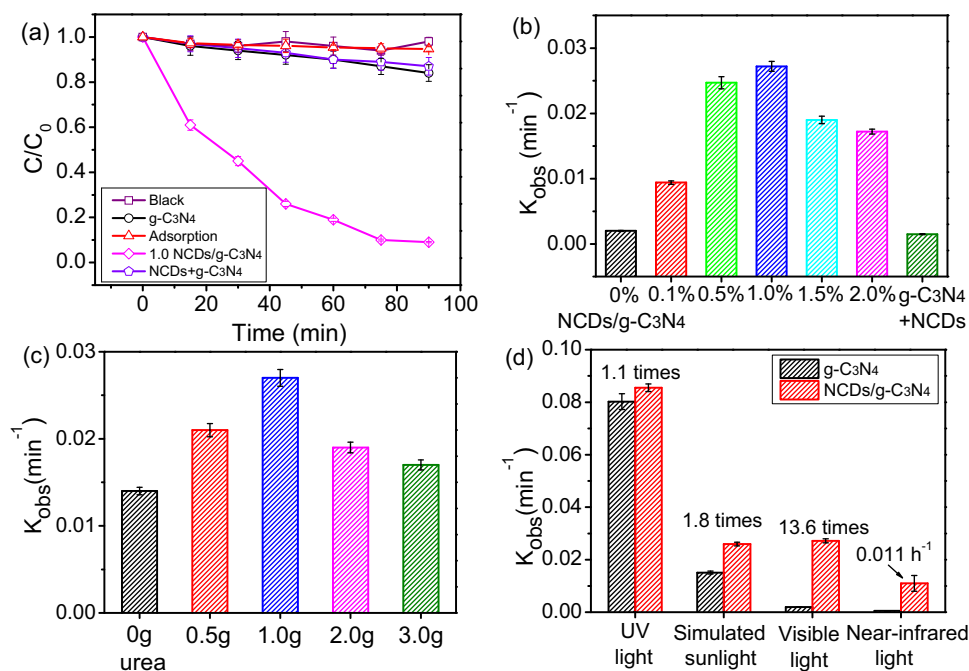


Fig. 5. (a) Photocatalytic activity of NCDs/g-C₃N₄ based on the photocatalytic degradation of IDM under visible light irradiation; (b) Kinetic rate constant of IDM degradation over different photocatalysts; (c) Kinetic rate constant of IDM degradation under visible light irradiation using NCDs/g-C₃N₄ prepared with different amount of urea. (d) Kinetic.

Although N doping may effectively improve electron transfer and lead to higher photolytic activity; excessive N atom concentrations can decrease effective surface contact areas between carbon and g-C₃N₄, which limits electron transfer and the conversion of optical energy [61].

3.2.4. Photocatalytic activity of NCDs/g-C₃N₄ under irradiation of different light sources

The photocatalytic activity of the NCDs/g-C₃N₄ composites has also been evaluated for the degradation of IDM under UV light, simulated sunlight, visible light, and near-infrared light irradiation. As shown in Fig. 5d, NCDs/g-C₃N₄ exhibited enhanced photocatalytic activity under all four light sources. It was revealed that the photocatalytic activity of 1.0 wt% NCDs/g-C₃N₄ was 1.1, 1.8, and 13.6 times higher than that of pristine g-C₃N₄ under UV light irradiation, simulated sunlight irradiation, and visible light irradiation, respectively. In addition, NCDs/g-C₃N₄ exhibited remarkable photocatalytic activity than pure g-C₃N₄ under near-infrared light irradiation. The NCDs/g-C₃N₄ composites showed an improved response under visible light and near-infrared irradiation. This difference may be attributed to the strong absorption properties of NCDs under short wavelength exposure, leading to the low photon absorption of g-C₃N₄. Moreover, NCDs cannot perform its up-converted PL property effectively under short wavelength irradiation, which limited the energy transfer from NCDs to g-C₃N₄.

3.2.5. Photocatalyst stability

To evaluate the recyclability of the NCDs/g-C₃N₄ composite, five cycling experiments were carried out for IDM photodegradation. As shown in Fig. 6a, 84% of the IDM was decomposed in 90 min on the fifth cycle, which was slightly lower than that of the first round (91%). From the FT-IR spectrum of the NCDs/g-C₃N₄ sample prior to and following five cycles Fig. 6b, it may be seen that there was no obvious change in characteristic stretching. The above results indicated that the NCDs/g-C₃N₄ showed high-stability under visible light irradiation due to the π - π stacking interactions between the NCDs and g-C₃N₄ [8].

3.3. Discussion of underlying photocatalyst mechanisms

3.3.1. Roles of reactive species

A series of reactive species (such as h^+ , $\text{O}_2^{\bullet-}$, and $\cdot\text{OH}$) are considered as being involved in the photocatalytic degradation of IDM during the photocatalytic process. It should be pointed out through the addition of IPA, BQ, Na₂C₂O₄, NaN₃, and K₂Cr₂O₇ performed different inhibitory effects on the photodegradation of IDM (Table 1), whereas IPA and NaN₃ induced a modest (<20%) inhibitory effect on the degradation of IDM. Nevertheless, Na₂C₂O₄, BQ, and K₂Cr₂O₇ demonstrated obvious inhibitory effects toward the degradation of IDM, with inhibition rates of 48.6%, 65.8%, and 84.7%, respectively. These results demonstrated that h^+ , $\text{O}_2^{\bullet-}$, and e^- played important roles in the degradation of IDM, while $\cdot\text{OH}$ and ${}^1\text{O}_2$ showed negligible effects. Previous studies confirmed that e^- may be captured by oxygen to generate $\text{O}_2^{\bullet-}$ [8,28,62]. A solution degassed with N₂ that contained Na₂C₂O₄, isopropanol, and NaN₃ has been investigated to verify the role of e^- during the photocatalytic process [28]. Only a slight decomposition of IDM was observed, revealing that e^- from the conduction band (CB) was preferentially involved in the degradation of IDM through the generation of $\text{O}_2^{\bullet-}$, rather than via e^- itself [63].

In this work, the formation of $\text{O}_2^{\bullet-}$ was monitored using NBD-Cl as a fluorescent probe. The obviously significant decomposition of NBD-Cl may be observed in Fig. 7. Moreover, the intensity of PL in the NBD-Cl product (reacting with $\text{O}_2^{\bullet-}$) at 550 nm (excited at 332 nm) was detected, which indicated the generation of $\text{O}_2^{\bullet-}$ during the photocatalytic process. The quantification of $\text{O}_2^{\bullet-}$ was then conducted by fluorescent analysis, employing a standard curve calibration (Fig. S9). The inset of Fig. 7 illustrates that longer irradiation durations initially increased and then decreased, the formation of $\text{O}_2^{\bullet-}$, which corresponds with previous reports [64,65]. In addition, 1.0 NCDs/g-C₃N₄ demonstrated the highest $\text{O}_2^{\bullet-}$ formation, which aligned well with the result of the photocatalytic degradation of IDM under visible light irradiation. This result revealed that the NCDs/g-C₃N₄ had efficient photocatalytic activity in the degra-

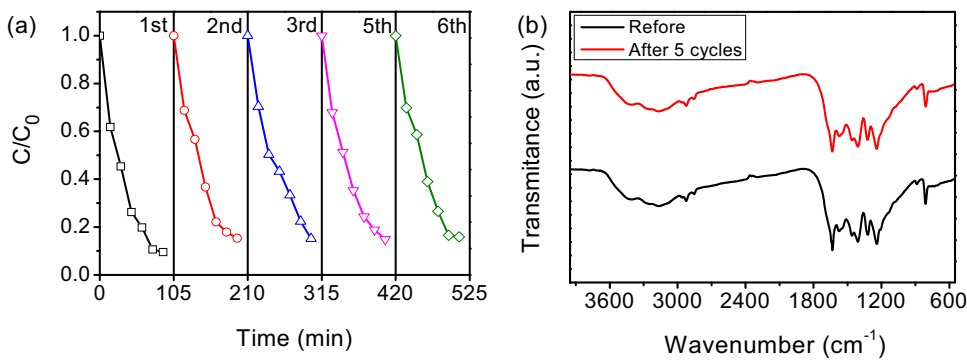


Fig. 6. (a) The repeated photocatalytic experiments for NCDs/g-C₃N₄; (b) the FT-IR spectrum of NCDs/g-C₃N₄ before and after 5cycles photocatalytic experiments.

Table 1
Scavengers used, RSs quenched and rate constants with quenched reactive species.

Quencher	RSs Quenched	K _{obs} (min ⁻¹)	Inhibition rate/%
Blank	\	(2.72 ± 0.10) × 10 ⁻²	0
IPA	•OH	(2.36 ± 0.05) × 10 ⁻²	13.1
BQ	O ₂ ^{•-}	(0.93 ± 0.03) × 10 ⁻²	65.8
NaN ₃	¹O ₂	(2.24 ± 0.08) × 10 ⁻²	17.5
K ₂ Cr ₂ O ₇	e ⁻	(0.41 ± 0.02) × 10 ⁻²	84.7
Na ₂ C ₂ O ₄	h ⁺	(1.43 ± 0.01) × 10 ⁻²	48.6
BQ + IPA + NaN ₃ + Na ₂ C ₂ O ₄ + N ₂	O ₂	(0.16 ± 0.01) × 10 ⁻²	94.2

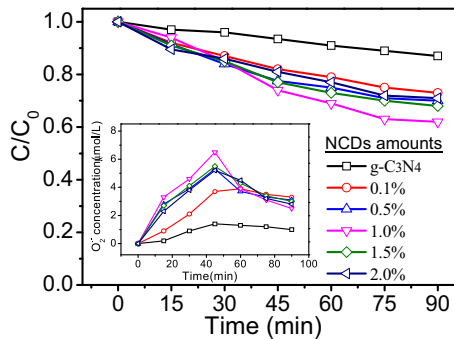


Fig. 7. Removal of NBD-Cl (Inset: the formation of superoxide radical anion) during NCDs/g-C₃N₄ photocatalytic degradation process.

dation of IDM through the generation of a large number of O₂^{•-} species.

3.3.2. Product identification

To test the proposed kinetics of the photocatalytic degradation of IDM, HPLC-MS/MS was employed to identify the generated intermediates. The elucidation of the structures of all intermediates was carried out based on both the analysis of the total ion chromatogram (TIC) and their corresponding fragmentation pattern. As shown in Fig. S10, nine products and IDM peaks were observed in the TIC, which were assigned to product A-I and IDM. Table S2 summarizes the overall fragment ions of IDM photocatalytic products, retention time, and the proposed corresponding molecular structures. Products with *m/z* 155 and *m/z* 218 molecular ions proved to be the cleavage products of amide bonds. Intermediates *m/z* 312, *m/z* 314, and *m/z* 342 arose from the cleavage of carboxyl from the acetic chain. Products with *m/z* 304 molecular ions were proposed as further hydroxylation products of *m/z* 312 (*m/z* 390 molecular ion was identified as the hydroxylation product of IDM, and *m/z* 366 was identified as the C2–C3 addition product).

The decrease of total organic carbon (TOC) was measured to evaluate the extent of mineralization during the degradation of IDM (Fig. 8). Following 90 min of irradiation, ca. 90.5% IDM was

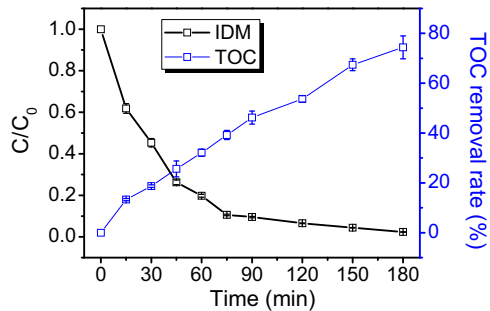


Fig. 8. The mineralization of IDM during NCDs/g-C₃N₄ photocatalytic degradation process.

decomposed, while only ca. 46.2% of the TOC was removed. The result indicated that more stable products might be generated during the photocatalytic process. However, ~74.4% of the TOC may be removed following 180 min of irradiation, which indicated that the IDM might be completely mineralized subsequent to longer NCDs/g-C₃N₄ irradiation times.

Furthermore, theoretical calculations were carried out in order to predict the reactive species attack positions [66]. The frontier electron densities (FEDs) data of the IDM molecules were calculated to predict the reaction sites for the RSs attack, as summarized in Table S3. The C19, C17, and C20 positions indicated higher FED²_{HOMO} + FED²_{LUMO} values, which revealed the high probability of •OH substituted reactions occurring at the chloro aromatic rings. The C17, C12, C5, C22, C16, and C2 atoms of IDM showed more positive point charge than others, which implied that C17, C12, C5, C22, C16, and C2 were likely to be attacked by O₂^{•-} via nucleophilic addition reactions. The prediction of potential attack positions by reactive species based on theoretical calculations was consistent with the results of the HPLC-MS/MS.

Potential photocatalytic IDM degradation pathways in aqueous media by NCDs/g-C₃N₄ hybrid photocatalysts under visible light irradiation were proposed, as illustrated in Fig. 9 and Text S2. In summary, product characterization indicated that the photocatalytic degradation of indomethacin involved (a) cleavage of the

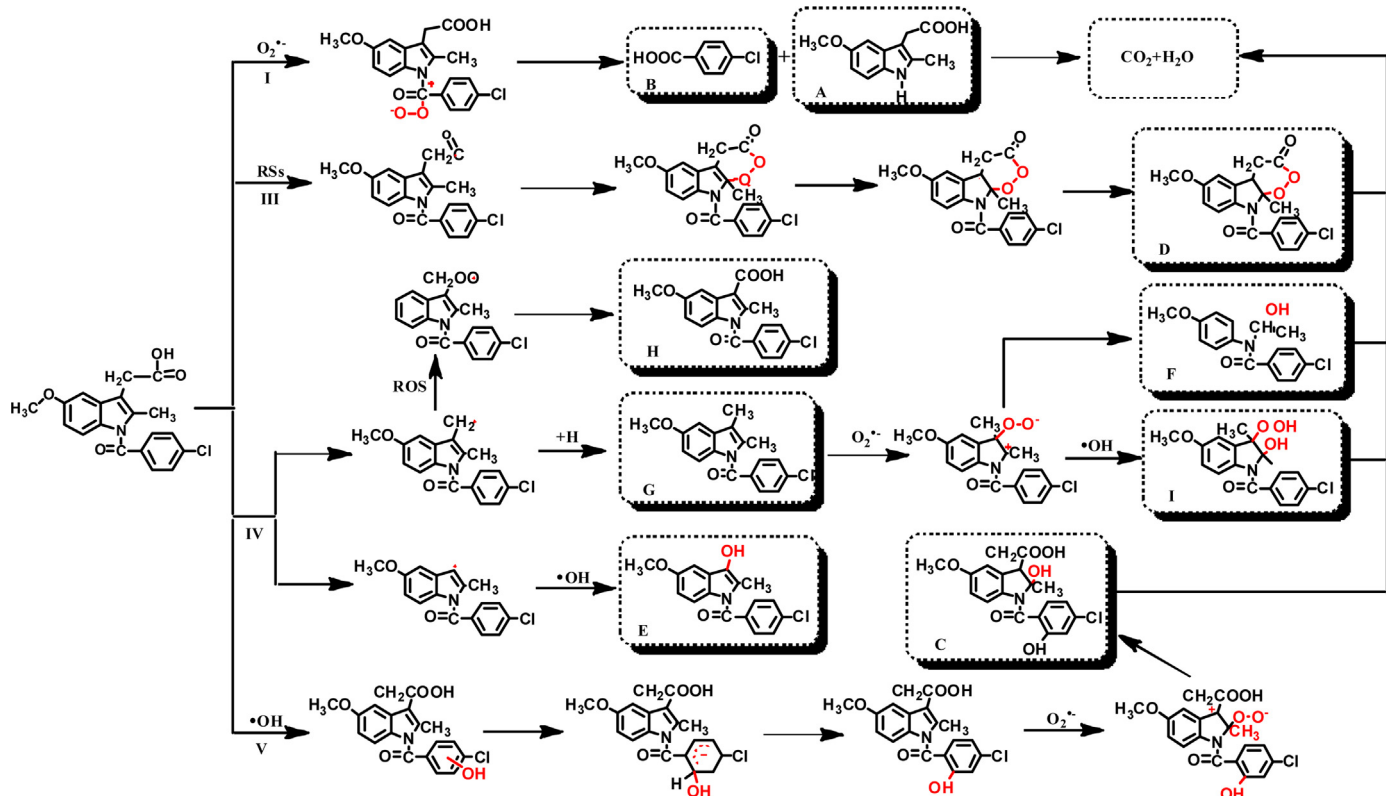


Fig. 9. Possible transformation pathways of IDM in NCDs/g-C₃N₄ aqueous solution under visible light irradiation.

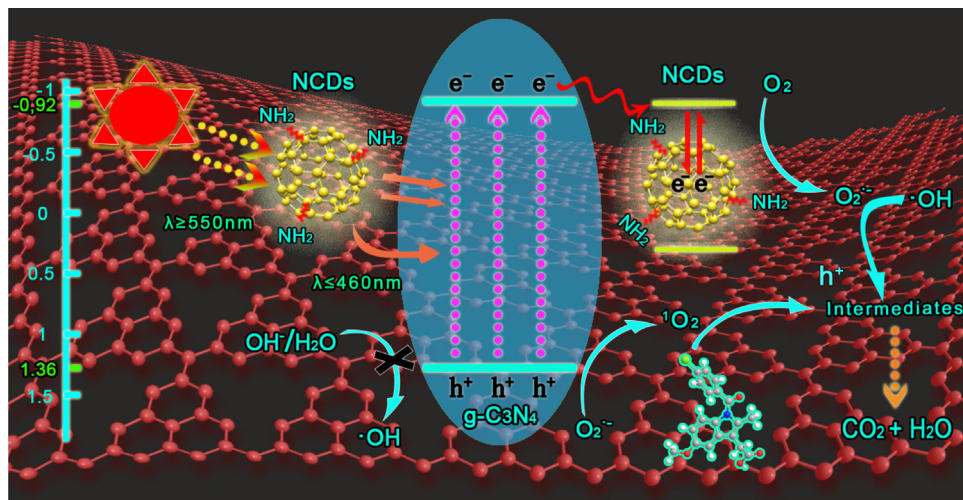


Fig. 10. Schematic illustration of the possible photocatalytic processes in the NCDs/g-C₃N₄ composite under visible light irradiation.

amide bond, (b) decarboxylation of the acetic chain, (c) addition reaction of the C2–C3 double bond, and (d) hydroxylation reaction of the chloro benzene ring.

3.3.3. Potential photocatalytic mechanisms

Based on the above results and the scientific literature [8,62,67], the potential photocatalytic mechanisms were proposed in Fig. 10. Under visible light irradiation, electron-hole pairs were formed with the photo-excitation of the g-C₃N₄ by absorbing light, with a wavelength <475 nm. Meanwhile, the >475 nm light wavelength could be converted to <475 nm light by NCDs due to its up-converted PL properties, which was subsequently absorbed by g-C₃N₄. Owing to the relatively strong electron affinity of N atoms

in NCDs, electrons in the CB can easily transfer to NCDs, leading to the efficient separation of electron-hole pairs. Subsequently, the electrons in NCDs may be captured by molecular oxygen, resulting in the generation of $O_2^{\bullet-}$ [4,28], which reacts with H⁺ to generate $\cdot OH$, meanwhile, it reacts with h⁺ to yield $^{1}O_2$ [68]. As the valence band (VB) position of g-C₃N₄ (+1.36 eV) is more negative than the standard redox potential of $\cdot OH/OH^-$ (+1.99 eV) and $\cdot OH/H_2O$ (+2.73 eV), the h⁺ from g-C₃N₄ cannot oxidize OH⁻ or H₂O to give $\cdot OH$ [69]. Consequently, the photocatalytic degradation of IDM in VB may be attributed to the direct reaction with h⁺ rather than $\cdot OH$. The production of RSs, such as $O_2^{\bullet-}$, h⁺, $^{1}O_2$, and $\cdot OH$ will attack IDM, leading to its efficient photocatalytic degradation and eventually complete mineralization.

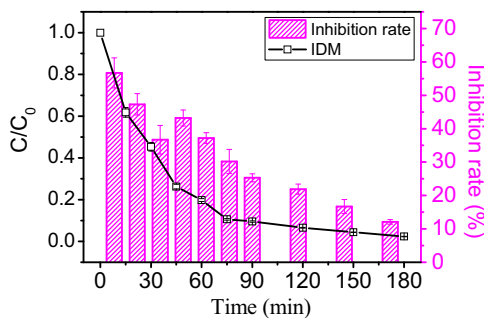


Fig. 11. Variation of toxicity by Microtox test, concentration of IDM during NCDs/g-C₃N₄ photocatalytic degradation process.

3.4. Toxicity evaluation

To investigate the potential risks of the photocatalytic degradation products of IDM, acute toxicity evaluations were conducted through the detection of the changes in the emissions of the luminescent bacteria *V. fischeri*, prior to and following treatment. Fig. 11 represents the variations in the photodegradation and inhibition rates of 4.0 mg/L IDM solutions in the presence of 1.0 g/L NCDs/g-C₃N₄ under visible light irradiation. As can be seen, the initial inhibition rate of 4.0 mg/L IDM was found to be 56.7%. During the photocatalytic treatment, the inhibition rate of treated solutions decreased to 36.7%. Subsequently, the toxicity increased and attained an inhibition rate of 43.2% when the irradiation duration was 45 min. This increase in toxicity may be attributed to the generation of additional toxic products during the photocatalysis of IDM. However, with further irradiation, the toxicity sharply decreased due to mineralization. Therefore, it may be confirmed that NCDs/g-C₃N₄ provides a very desirable performance in toxicity reduction and mineralization of IDM in engineered systems that are employed for potable water and wastewater treatment under visible light irradiation.

4. Conclusions

In conclusion, a NCDs/g-C₃N₄ composite photocatalyst was successfully synthesized via a facile polymerization method. Characterization results confirmed the formation of the NCDs/g-C₃N₄ composite, in which the NCDs nanoparticles were securely attached to the g-C₃N₄ lamellar structure via π - π stacking interactions. In comparison to pristine g-C₃N₄ and CDs/g-C₃N₄, the NCDs/g-C₃N₄ displayed enhanced photocatalytic activity in the degradation of IDM under wide spectrum (near-infrared light, visible light, simulated sunlight, and UV light). Of these samples, NCDs/g-C₃N₄ exhibited an improved visible light and near-infrared light response in contrast to other light sources. This enhanced photocatalytic performance might be attributed to a unique up-converted PL property, efficient charge separation, and bandgap narrowing of NCDs. An analysis of reactive species confirmed that O₂^{•-} and h⁺ played key roles during the photocatalytic degradation of IDM. Based on the identification of intermediates using HPLC/MS, and the predictions of reactive sites via FEDs, the photocatalytic IDM degradation pathways were proposed. The IDM degradation pathways involved decarboxylation, hydroxylation, as well as the addition and cleavage of indole rings. In addition, a toxicity assessment showed that the toxicity of IDM solutions may be reduced by NCD/g-C₃N₄ subsequent to sufficient visible light irradiation times. Hence, our results demonstrated that the NCDs/g-C₃N₄ photocatalytic process is a promising technology for IDM toxicity reduction and mineralization.

Acknowledgements

This work was supported by the National Natural Science Foundation of China (Nos. 21377031 and 21677040), the Innovative Team Program of High Education of Guangdong Province (2015KCXTD007).

Appendix A. Supplementary data

Supplementary data associated with this article can be found, in the online version, at <http://dx.doi.org/10.1016/j.apcatb.2017.02.024>.

References

- [1] F. Dong, L. Wu, Y. Sun, M. Fu, Z. Wu, S.C. Lee, *J. Mater. Chem.* 21 (2011) 15171–15174.
- [2] D. Lu, G. Zhang, Z. Wan, *Appl. Surf. Sci.* 358 (2015) 223–230.
- [3] X. Wang, S. Blechert, M. Antonietti, *ACS Catal.* 2 (2012) 1596–1606.
- [4] J. Ma, C. Wang, H. Hong, *Appl. Catal. B Environ.* 184 (2016) 28–34.
- [5] J. Liu, Y. Yang, N. Liu, Y. Liu, H. Huang, Z. Kang, *Green Chem.* 16 (2014) 4559–4565.
- [6] J. Wang, R. Liu, C. Zhang, G. Han, J. Zhao, B. Liu, C. Jiang, Z. Zhang, *RSC Adv.* 5 (2015) 86803–86810.
- [7] L. Liu, Y. Qi, J. Hu, Y. Liang, W. Cui, *Appl. Surf. Sci.* 351 (2015) 1146–1154.
- [8] Z. Hui, L. Zhao, F. Feng, L.H. Guo, B. Wan, Y. Yu, *Appl. Catal. B Environ.* 180 (2016) 656–662.
- [9] R. Miao, Z. Luo, W. Zhong, S.Y. Chen, T. Jiang, B. Dutta, Y. Nasr, Y. Zhang, S.L. Suib, *Appl. Catal. B Environ.* 189 (2016) 26–38.
- [10] Q. Huang, X. Lin, C. Lin, Y. Zhang, S. Hu, C. Wei, *RSC Adv.* 5 (2015) 54102–54108.
- [11] S. Pandey, A. Mewada, M. Thakur, S. Pillai, R. Dharmatti, C. Phadke, M. Sharon, *RSC Adv.* 4 (2013) 1174–1179.
- [12] J. Liu, Y. Liu, N. Liu, Y. Han, X. Zhang, H. Huang, Y. Lifshitz, S.T. Lee, J. Zhong, Z. Kang, *Science* 46 (2015) 970–974.
- [13] S. Fang, Y. Xia, K. Lv, Q. Li, J. Sun, M. Li, *Appl. Catal. B Environ.* 185 (2015) 225–232.
- [14] Y. Guo, P. Yao, D. Zhu, C. Gu, *J. Mater. Chem. A* 3 (2015) 13189–13192.
- [15] Y. Hong, Y. Meng, G. Zhang, B. Yin, Y. Zhao, W. Shi, C. Li, *Sep. Purif. Technol.* 171 (2016) 229–237.
- [16] J. Yu, C. Xu, Z. Tian, Y. Lin, Z. Shi, *New J. Chem.* 40 (2016) 2083–2088.
- [17] Y. Sun, Z. Zhang, A. Xie, C. Xiao, S. Li, F. Huang, Y. Shen, *Nanoscale* 7 (2015) 13974–13980.
- [18] E.N. Evgenidou, I.K. Konstantinou, D.A. Lambropoulou, *Sci. Total Environ.* 505 (2015) 905–926.
- [19] T. Qiao, Z. Yu, X. Zhang, D.W. Au, *J. Environ. Monit. Jem* 13 (2011) 3097–3103.
- [20] P. Chen, F.L. Wang, K. Yao, J.S. Ma, F.H. Li, W.Y. Lv, G.G. Liu, *Bull. Environ. Contam. Toxicol.* 96 (2016) 203–209.
- [21] C.I. Kosma, D.A. Lambropoulou, T.A. Albanis, *Sci. Total Environ.* 466–467 (2014) 421–438.
- [22] C. Ort, M.G. Lawrence, J. Reungoat, J.F. Mueller, *Sci. Environ. Technol.* 44 (2010) 6289–6296.
- [23] L. Nováková, L. Matysová, L. Havlíková, P. Solich, *J. Pharm. Biomed. Anal.* 37 (2005) 899–905.
- [24] S. Qu, X. Wang, Q. Lu, X. Liu, L. Wang, *Angew. Chem. Int. Ed.* 51 (2012) 12381–12384 (12384).
- [25] V. Kitsiou, N. Filippidis, D. Mantzavinos, I. Poulios, *Appl. Catal. B Environ.* 86 (2009) 27–35.
- [26] A. Chatzitakis, C. Berberidou, I. Paspaltsis, G. Kyriakou, T. Sklaviadis, I. Poulios, *Water Res.* 42 (2008) 386–394.
- [27] A.M. Braun, M.T. Maurette, E. Oliveros, *Photochemical Technology*, Wiley, 1991.
- [28] G.Y. Li, X. Nie, J.Y. Chen, Q. Jiang, T.C. An, P.K. Wong, H.M. Zhang, H.J. Zhao, H. Yamashita, *Water Res.* 86 (2015) 17–24.
- [29] H. Xiao, J. Zhu, A. Thomas, *RSC Adv.* 5 (2015) 105731–105734.
- [30] T. Fotiou, T.M. Triantis, T. Kaloudis, K.E. O’Shea, D.D. Dionysiou, A. Hiskia, *Water Res.* 90 (2016) 52–61.
- [31] R.O. Olojo, R.H. Xia, J.J. Abramson, *Anal. Biochem.* 339 (2005) 338–344.
- [32] M.I. Heller, P.L. Croot, *Anal. Chim. Acta* 667 (2012) 1–13.
- [33] B.S. Institution, ISO 11348-2. Water quality. Determination of the inhibitory effect of water samples on the light emission of *Vibrio fischeri* (Luminescent bacteria test). Part 2. Method using liquid-dried bacteria.
- [34] Y. Ji, L. Zhou, C. Ferronato, X. Yang, A. Salvador, C. Zeng, J.M. Chovelon, *J. Photochem. Photobiol. A Chem.* 254 (2013) 35–44.
- [35] H.S. Wahab, T. Bredow, S.M. Aliwi, *Surf. Sci.* 603 (2009) 664–669.
- [36] J. Yu, C. Xu, Z. Tian, Y. Lin, Z. Shi, *New J. Chem.* 40 (2015) 2083–2088.
- [37] H. Wang, P. Sun, C. Shan, J. Wu, L. Gao, Y. Wang, X. Dai, Q. Yi, G. Zou, *Nanoscale Res. Lett.* 11 (2016) 1–6.
- [38] J. Zhang, X. Zhang, S. Dong, X. Zhou, S. Dong, *J. Photochem. Photobiol. A Chem.* 325 (2016) 104–110.
- [39] W. Lu, Y. Li, R. Li, S. Shuang, C. Dong, Z. Cai, *ACS Appl. Mater. Interfaces* (2016).

- [40] T. Edison, R. Atchudan, J.J. Shim, S. Kalimuthu, B.C. Ahn, Y.R. Lee, J. Photochem. Photobiol. B-Biol. 158 (2016) 235–242.
- [41] X. Dong, Y. Su, H. Geng, Z. Li, C. Yang, X. Li, Y. Zhang, J. Mater. Chem. C 2 (2014) 7477–7481.
- [42] P. Chen, F. Wang, Z.F. Chen, Q. Zhang, Y. Su, L. Shen, K. Yao, Y. Liu, Z. Cai, W. Lv, Appl. Catal. B Environ. 204 (2016) 250–259.
- [43] Q. Li, M. Zhou, Q. Yang, Q. Wu, J. Shi, A. Gong, M. Yang, Chem. Mater. 28 (2016) 8221–8227.
- [44] J. Yu, N. Song, Y.K. Zhang, S.X. Zhong, A.J. Wang, J. Chen, Sens. Actuators B Chem. 214 (2015) 29–35.
- [45] L. Wang, F. Ruan, T. Lv, Y. Liu, D. Deng, S. Zhao, H. Wang, S. Xu, J. Lumin. 158 (2015) 1–5.
- [46] Y. Feng, K. Lu, M. Liang, X. Guo, S. Gao, E.J. Petersen, Water Res. 84 (2015) 49–57.
- [47] M. Xu, G. He, Z. Li, F. He, F. Gao, Y. Su, L. Zhang, Z. Yang, Y. Zhang, Nanoscale 6 (2014) 10307–10315.
- [48] D. Qu, M. Zheng, P. Du, Y. Zhou, L. Zhang, D. Li, H. Tan, Z. Zhao, Z. Xie, Z. Sun, Nanoscale 5 (2013) 12272–12277.
- [49] S. Xu, H. Yun, M. Zheng, C. Wei, Appl. Catal. B Environ. 182 (2016) 587–597.
- [50] J. Hong, X. Xia, Y. Wang, R. Xu, J. Mater. Chem. 22 (2012) 15006–15012.
- [51] J. Pan, Y. Sheng, J. Zhang, J. Wei, P. Huang, X. Zhang, B. Feng, J. Mater. Chem. A 2 (2014), 1–1.
- [52] X.H. Li, J. Zhang, X. Chen, A. Fischer, A. Thomas, M. Antonietti, X. Wang, Chem. Mater. 23 (2011) 4344–4348.
- [53] W.J. Ong, L.L. Tan, S.P. Chai, S.T. Yong, Chem. Commun. 51 (2015) 858–861.
- [54] Z. Ding, X. Chen, M. Antonietti, X. Wang, Chemsuschem 4 (2011) 274–281.
- [55] A.P. Dementjev, A.D. Graaf, M.C.M.V.D. Sanden, K.I. Maslakov, A.V. Naumkin, A.A. Serov, Diam. Relat. Mater. 9 (2000) 1904–1907.
- [56] S.T. Kochuveedu, J.J. Yu, Y.H. Jang, W.J. Lee, M.A. Cha, H. Shin, S. Yoon, S.S. Lee, O.K. Sang, K. Shin, Green Chem. 13 (2011) 3397–3405.
- [57] Y. Guo, J. Li, Z. Gao, X. Zhu, Y. Liu, Z. Wei, W. Zhao, C. Sun, Appl. Catal. B Environ. 192 (2016) 57–71.
- [58] Y. Li, Y. Zhao, H. Cheng, Y. Hu, G. Shi, L. Dai, L. Qu, J. Am. Chem. Soc. 134 (2011) 15–18.
- [59] K. Gong, F. Du, Z. Xia, M. Durstock, L. Dai, Science 323 (2009) 760–764.
- [60] D. Yu, Q. Zhang, L. Dai, J. Am. Chem. Soc. 132 (2010) 15127–15129.
- [61] H.C. Chang, S.H. Park, S.I. Woo, Int. J. Hydrogen Energy 37 (2012) 4563–4570.
- [62] J. Xia, J. Di, H. Li, X. Hui, H. Li, S. Guo, Appl. Catal. B Environ. 181 (2016) 260–269.
- [63] H.S. Fang, Y.P. Gao, G.Y. Li, J.B. An, P.K. Wong, H.Y. Fu, S.D. Yao, X.P. Nie, T.C. An, Sci. Environ., Technol. 47 (2013) 2704–2712.
- [64] A. Ikhlaq, D.R. Brown, B. Kasprzyk-Hordern, Appl. Catal. B Environ. 129 (2013) 437–449.
- [65] T. Xu, R. Zhu, J. Zhu, X. Liang, Y. Liu, Y. Xu, H. He, Catal. Sci. Technol. 6 (2016) 4116–4123.
- [66] M. Carrier, C. Guillard, M. Besson, C. Bordes, H. Chermette, J. Phys. Chem. A 113 (2009) 6365–6374.
- [67] J. Chen, H. Che, K. Huang, C. Liu, W. Shi, Appl. Catal. B Environ. 192 (2016) 134–144.
- [68] J. Ng, X. Wang, D.D. Sun, Appl. Catal. B Environ. 110 (2011) 260–272.
- [69] D. Wu, B. Wang, W. Wang, T. An, G. Li, T.W. Ng, H.Y. Yip, C. Xiong, H.K. Lee, P.K. Wong, J. Mater. Chem. A 3 (2015) 15148–15155.